GAS6 and AXL promote insulin resistance by rewiring insulin signaling and increasing insulin receptor trafficking to late endosomes

Céline Schott[1,2,7], Amélie Germain[1,2,7], Julie Lacombe[1], Denis Faubert[3], Jonathan Boulais[4], Jean-François Côté [2,4,5,6] and Mathieu Ferron[1,2,5,6]

1. Molecular Physiology Research Unit, Institut de Recherches Cliniques de Montréal (IRCM), Montréal, Québec, Canada
2. Programme de Biologie Moléculaire, Université de Montréal, Montréal, Québec, Canada
3. Mass Spectrometry and Proteomics Platform, Institut de Recherches Cliniques de Montréal (IRCM), Montréal, Canada.
4.Cytoskeletal Organization and Cell Migration Research Unit, Institut de Recherches Cliniques de Montréal (IRCM), Montréal, Québec, Canada
5. Département de Médicine, Université de Montréal, Montréal, Québec, Canada
6. Division of Experimental Medicine, McGill University, Montréal, Québec, Canada
7. These authors contributed equally

Running Head: GAS6 inhibits insulin signaling.

Keywords: GAS6; AXL; muscle; insulin resistance; glucose metabolism; endosomes

Corresponding author:
Mathieu Ferron, PhD
Institut de Recherches Cliniques de Montréal
110 Ave. des Pins O.
Montréal, QC,
H2W 1R7, Canada
Phone: 514-987-5754
Email: mathieu.ferron@ircm.qc.ca

4955 words, 8 Figures

ABSTRACT

Growth-arrest specific 6 (GAS6) is a secreted protein that acts as a ligand for TAM receptors (TYRO3, AXL and MERTK). In humans, GAS6 circulating levels and genetic variations in *GAS6* are associated with hyperglycemia and increased risk of type 2 diabetes. However, the mechanisms by which GAS6 influences glucose metabolism are not understood. Here, we show that *Gas6* deficiency in mice increases insulin sensitivity and protects from diet-induced insulin resistance. Conversely, increasing GAS6 circulating levels is sufficient to reduce insulin sensitivity *in vivo*. Recombinant GAS6 inhibits the activation of the insulin receptor (IR) and reduces insulin response in muscle cells. Mechanistically, AXL heterodimerizes with the IR, while GAS6 reprograms signaling pathways downstream of IR. This results in increased trafficking of the IR to Rab7a-positive late endosomes following insulin treatment. Together, these results contribute to a better understanding of the cellular and molecular mechanisms by which GAS6 and AXL influence insulin sensitivity.

ARTICLE HIGHLIGHTS

- GAS6 deficient mice are characterized by improved glucose tolerance, increased insulin sensitivity and are protected from diet-induced insulin resistance.
- The GAS6 receptor AXL is expressed in muscle cells and physically interacts with the insulin receptor.
- GAS6 reprograms insulin signaling by modulating the phosphorylation of proteins implicated in endocytosis, vesicle-mediated transport, and membrane trafficking.
- AXL promotes insulin receptor trafficking to late endosome following insulin treatment.

INTRODUCTION

At the root of the pathophysiology of type 2 diabetes (T2D) lies insulin resistance, an insufficient response to insulin in skeletal muscle, white adipose tissue, and liver. In normal conditions, insulin mediates its actions through the binding of the insulin receptor (IR), triggering IR dimerization and autophosphorylation of its tyrosine kinase domain. These molecular events result in the recruitment and phosphorylation of insulin receptor substrates (IRS) proteins leading to the activation of the phosphatidylinositol 3-kinase (PI3K)/protein kinase B (AKT) pathway that plays a critical role in the molecular response to insulin [1]. Alterations in IR and PI3K/AKT activation or phosphorylation in response to insulin impact several cellular pathways including glucose uptake [2]. In addition, a reduction in the level of activation of the insulin signaling cascade in muscle has been associated with insulin resistance and contributes to the development of T2D [3-5]. However, the cellular mechanisms involved in the development of muscle insulin resistance are still not fully understood.

Growth-arrest specific 6 (GAS6) is a secreted protein initially identified as upregulated in growth-arrested fibroblasts [6]. GAS6 is composed of an N-terminal Gla domain containing γ-carboxyglutamic acids, four central epidermal growth factor-like domains and two laminin G-like (LG) domains [7-9]. GAS6 functions as a ligand for the TAM family of receptor tyrosine kinases (RTK), which includes 3 members: TYRO3, AXL and MERTK [10]. Protein S (PROS), which functions as an anticoagulant factor, shares 44% of its amino acid sequence with GAS6. However, GAS6 and PROS may have different functions *in vivo* given that mice lacking *Pros1* dies in utero from hemorrhages, while *Gas6*$^{-/-}$ mice are viable and do not suffer from spontaneous bleeding or thrombosis [11, 12]. Recent studies have established that only GAS6 can activate

AXL, while TYRO3 and MERTK act as both PROS and GAS6 receptors [13, 14], suggesting that the non-redundant functions of GAS6 are mediated by AXL. TAM receptors have been implicated in several homeostatic functions in adult mice including spermatogenesis, clearance of apoptotic cells, suppression of inflammation, and platelet activation [15-18], but are also involved in tumor progression and metastasis [19, 20]. Nevertheless, the physiological functions of GAS6 remains unclear, since mice lacking *Gas6* are apparently devoid of phenotype under normal conditions [12, 21].

Studies in humans suggest a potential role for GAS6 and AXL in insulin sensitivity, glucose homeostasis and T2D [22-24]. Serum levels of GAS6 were found to be elevated in obese adolescents compared to lean subjects and circulating levels of GAS6 were strongly correlated with insulin resistance in this population [24]. Genome-wide association studies (GWAS) have identified a positive association between non-coding single-nucleotide polymorphisms (SNP) in the human *GAS6* gene and the circulating levels of glycated hemoglobin (HbA1c), a marker of hyperglycemia [25, 26]. Although these data suggest that GAS6 may play a role in the development of insulin resistance and T2D in humans, the physiological and molecular mechanisms through which GAS6 and its receptor(s) might influence these metabolic disorders are currently unknown. Likewise, the cell type(s) targeted by GAS6 and regulating glucose metabolism remain to be identified.

Here, we first show that the absence of GAS6 in mice on two different inbred genetic backgrounds improves glucose tolerance and insulin sensitivity, without affecting insulin secretion, body weight or energy expenditure. Next, we establish that AXL interacts with IR in an insulin-dependent manner and, through quantitative phosphoproteomics, we demonstrate that

GAS6 profoundly modifies insulin signaling in muscle cells leading to increased insulin receptor trafficking to late endosomes. This study uncovers a crosstalk between GAS6 and insulin -signaling and provide the basis of a molecular mechanism by which GAS6 promotes insulin resistance and T2D.

RESEARCH DESIGN AND METHODS

Mice

Gas6$^{-/-}$ mice on a C57BL/6J genetic background were generously provided by Dr Peter Carmeliet (The Center for Transgene Technology and Gene Therapy, Flanders Interuniversity Institute of biotechnology, Belgium) [12]. *Gas6*$^{-/-}$ mice on a FVB/N genetic background were previously described by us [20]. *ApoE-Gas6*^{Tg} transgenic mice were generated in our laboratory as described in Supplemental Material. All strains were maintained in an IRCM specific pathogen-free animal facility under 12-hour dark/12-hour light cycles. Mice were fed ad libitum a normal chow diet (Teklad global 18% protein rodent diet; 2918; Envigo), unless otherwise specified. Male mice were used in all experiments.

Cell Lines

The C2C12, HEK293, HEK293 Flp-In T-Rex cells expressing or not AXL-BirA*-Flag and L6-GLUT4myc cells are described in Supplemental Material.

Metabolic Analysis

For glucose tolerance tests (GTT), mice were fasted 16 hours and injected intraperitoneally (i.p.) with 2 g/kg glucose. For insulin tolerance test (ITT), mice were fasted 6 hours, injected i.p. with recombinant insulin (Humulin R Lilly) (0.6 U/kg for *Gas6*$^{-/-}$ mice or 0.75 U/kg for *ApoE-Gas6*^{Tg} transgenic mice). For pyruvate tolerance test, mice were fasted 16 hours and injected i.p. with sodium pyruvate (2 g/kg). Blood glucose levels were measured using a Bravo glucometer (EndoMedical Inc.). In vivo glucose stimulated insulin secretion test (GSIS) were performed after 16 hours of fasting and i.p. injection with 3 g/kg glucose. Serum insulin was measured with a commercial insulin ELISA kit (Mercodia).

Mouse physiological parameters were measured using an 8-chamber Promethion Continuous Metabolic System (Sable Systems International) as we previously reported [27]. Body composition was evaluated with a body composition analyzer (echo-MRI). When indicated, mice were fed a 60% high-fat high-sucrose diet (D12331; Research Diets) for 12 weeks starting from 5 weeks of age and fasted for 6 hours for GTT (1 g/kg glucose) and ITT (0.75 U/kg insulin).

DNA Constructs

All constructs were generated by PCR using primers included in **Supplemental Table 1** and as described in Supplemental Material.

Production and Purification of Recombinant GAS6

Carboxylated and uncarboxylated mouse Gas6 production, purification and quantification were performed as described in Supplemental Material.

Treatment with GAS6

For 15-minute GAS6 stimulation, C2C12 cells were starved overnight in DMEM media with 0.5% FBS. After two PBS 1X washes, cells were cultured for 2h in serum-free medium supplemented with 10 mM of HEPES pH 7.4, and 0.1% BSA and stimulated for 15 minutes with 200 ng/ml of recombinant carboxylated or uncarboxylated GAS6. For 8 and 24-hour GAS6 treatment, C2C12 and L6-GLUT4myc cells were incubated in serum-free medium with or without recombinant GAS6 (200ng/ml).

Co-Immunoprecipitation and Western Blot

HEK293 cells were transfected with pcDNA5-AXL-BirA*-Flag and pcDNA3-IR-HA and processed as described in Supplementary Material. Antibodies used for western blot are listed in **Supplemental Table 2**.

Streptavidin Pull-Down

HEK293 Flp-In T-Rex cells expressing AXL-BirA*-Flag were cultured during 24 hours with biotin (50µM) and tetracycline (1µg/ml), then cultured in 0.5% FBS DMEM overnight and incubated in serum-free medium (with 0.1% BSA and 10 mM HEPES) for 2 hours followed by 15-minute stimulation with insulin (100 nM). Streptavidin pull-down was performed as described in Supplementary Material.

Immunofluorescence Confocal Microscopy

HEK293 cells were transfected with pcDNA5-AXL-BirA*-Flag and/or pmScarlet-C1-Rab7 and processed as described in Supplementary Material. Antibodies used for immunofluorescence are listed in **Supplemental Table 2**. Images were acquired with Zeiss LSM700 confocal microscope with a 63X oil objective. We used Image J software to quantify Insulin Receptor (IR) and Rab7 localization. For each different condition, IR signal intensity (Alexa488) was measured across the cell and represented as a distance from the nucleus to the plasma membrane (n=30 cells per condition, from 3 independent experiments).

Gene Expression

Tissue and cell total RNA extraction and isolation were performed as described in Supplemental Material.

Protein Digestion for Phosphoproteome Analysis

C2C12 cells were incubated in serum-free medium with or without recombinant GAS6 (200ng/ml) for 24 hours and treated or not with insulin (100 nM) for 15 minutes. Protein extract were digested with benzonase as described in Supplementary Material.

Isobaric Peptide Labeling and LC-MS/MS Analysis

Protein digests were labelled using the 6-plex tandem mass tag reagent (Thermo Fisher Scientific) and analyzed by LC-MS/MS as described in Supplementary Material.

Bioinformatics

We considered as modulated phosphosites those showing a normalized Log2 (≤ -0.5 or ≥ 0.5) between two given conditions and $P < 0.05$. Detailed analysis of the phophopeptides is available in Supplemental Tables 3-6: https://figshare.com/s/43f5bf99204c1d928e05. Reactome pathway analyses were performed to functionally annotate proteins using Gene Set Enrichment Analysis (GSEA) with an FDR threshold of 0.05. Graphical network representations of protein-protein interaction were performed with the STRING app (11.5) in Cytoscape (3.9.1).

Statistics

Statistical analyses were performed using GraphPad Prism software as described in Supplementary Material.

Data and Resource Availability

The data and resources generated and/or analyzed during the current study are available from the corresponding author upon reasonable request.

RESULTS

GAS6 deficiency improves glucose tolerance and insulin sensitivity in mice fed a normal chow diet

To determine GAS6 function in glucose homeostasis, we characterized the metabolic phenotype of 3-month-old *Gas6*$^{-/-}$ male mice fed a standard chow diet on two inbred genetic backgrounds: FVB/N and C57BL/6J. These two strains were selected because they are both widely used in metabolic studies but have significant differences in whole-body glucose metabolism [28]. When compared to control littermates on the same genetic background, *Gas6*$^{-/-}$ mice did not display any differences in energy expenditure parameters, physical activity, body weight and food intake (**Fig.S1A-P**). However, on both genetic backgrounds, *Gas6*$^{-/-}$ mice have significantly reduced serum glucose levels in fed conditions (**Fig. 1A-B**) or after a glucose load as assessed through glucose tolerance tests (GTTs) (**Fig.1C-D**).

Insulin tolerance tests (ITT) suggested that *Gas6*$^{-/-}$ mice on FVB/N or C57BL/6J backgrounds had improved insulin sensitivity (**Fig.1E-F**). Glucose-stimulated insulin secretion tests (GSIS) showed that *Gas6*$^{-/-}$ mice had normal insulin secretion in response to glucose (**Fig.1G-H**). Gluconeogenesis from pyruvate was not significantly affected in *Gas6*$^{-/-}$ mice, as assessed by pyruvate tolerance tests (PTT) (**Fig.S1Q-R**). Together, these data suggest that GAS6-deficiency improves glucose tolerance by affecting insulin sensitivity, but not insulin secretion or gluconeogenesis.

Gas6-deficient mice are protected from diet-induced insulin resistance

We next investigated whether GAS6 deficiency could have beneficial effects on glucose metabolism in a model of obesity induced by a high-fat and high-sucrose diet (HFHS). This study was performed only in mice on C57BL/6J genetic background, since this inbred strain is more susceptible to diet-induced obesity compared to FVB/N [29]. Twelve weeks of HFHS feeding equally affected body weight, body composition (fat and lean mass) and the weight of epididymal and subcutaneous white adipose tissues (eWAT and scWAT) in *Gas6*$^{+/+}$ and *Gas6*$^{-/-}$ mice (**Fig.2A-E**). Obesity is associated with WAT inflammation characterized by an increased number of activated macrophages that contribute to insulin resistance in this tissue [30] and TAM receptors have been previously implicated in immune cell functions [31, 32]. However, although the number and area of F4/80 positive macrophages in WAT following the HFHS diet was increased as expected, no significant impact of the genotype was observed (**Fig.S2A-B**).

Following a 6h fast, control mice (*Gas6*$^{+/+}$) under HFHS diet displayed a significant increase in blood glucose in comparison with those fed a chow diet (**Fig.2F**). In contrast, fasting glycemia in *Gas6*$^{-/-}$ mice did not increase following an HFHS diet feeding and remained comparable with control chow-fed mice (**Fig.2F**). Strikingly, glucose tolerance was similar between *Gas6*$^{-/-}$ mice fed an HFHS diet and *Gas6*$^{+/+}$ mice fed a chow diet, whereas *Gas6*$^{+/+}$ mice fed an HFHS diet were significantly more glucose intolerant (**Fig.2G**). Insulin sensitivity was also markedly improved in *Gas6*$^{-/-}$ mice fed an HFHS diet compared to *Gas6*$^{+/+}$ littermates fed with the same diet (**Fig.2H**). Insulin secretion following a glucose load (GSIS) tended to be higher in some of the *Gas6*-deficient mice under an HFHS diet, but this difference did not reach statistical significance (**Fig.2I**). Altogether, these data indicate that the inactivation of *Gas6* can prevent

insulin resistance and glucose intolerance induced by HFHS diet without affecting body weight and composition, or insulin secretion.

Increasing GAS6 circulating levels reduces insulin sensitivity in mice

We then aimed to determine if increasing circulating GAS6 levels is sufficient to decrease insulin sensitivity. For that purpose, we generated a transgenic gain-of-function mouse model in which the liver-specific regulatory sequences of the human *APOE* gene [33, 34] were used to achieve ectopic expression of a Myc-6×His-tagged version of mouse GAS6 in hepatocytes and secretion in blood (**Fig.3A**). The liver was selected as a site of expression for two reasons. First, overexpression of secreted proteins in hepatocytes using the human *APOE* promoter was previously shown to result in significantly increased circulating levels of these proteins. Second, the liver being a major site of production for vitamin K-dependent proteins such as prothrombin, GAS6 ectopically produced by this organ will be fully γ-carboxylated and active.

ApoE-Gas6^{Tg} mice were generated and maintained on a pure C57BL/6J genetic background. Quantitative PCR (qPCR) confirmed that *Gas6* mRNA levels were ~18 times higher in the liver of the *ApoE-Gas6*^{Tg} mice compared to wild type (WT) littermate mice (**Fig.3B**). *Gas6* expression was unaffected in other tissues such as skeletal muscle, epididymal white adipose tissue (eWAT) or brown adipose tissue (BAT). Circulating levels of GAS6, measured using a specific ELISA assay, were approximately 8 times higher in the transgenic animals as compared to WT (**Fig.3C**).

Systemic elevation of GAS6 had no impact on body weight at 3 or 6 months of age compared to WT mice fed a standard chow diet (**Fig.3D**). At 3 months of age, *ApoE-Gas6*^{Tg} mice did not

show any changes in glycemia, in fed or fasted conditions (**Fig.3E**). However, a significantly reduced insulin sensitivity was detected at the same age in *ApoE-Gas6*^{Tg} mice (**Fig.3F**). Six-month-old *ApoE-Gas6*^{Tg} mice displayed a significantly increased glycemia in fed conditions and after a 5h fasting period (**Fig. 3G**), while insulin sensitivity was still reduced compared to WT mice (**Fig.3H**). Glucose tolerance was not affected in *ApoE-Gas6*^{Tg} mice (**Fig. S3A-B**), suggesting that reduced insulin sensitivity was counterbalanced by glucose disposal mechanisms independently of insulin [35]. Therefore, increasing GAS6 circulating levels is sufficient to reduce insulin sensitivity *in vivo*.

AXL is expressed and activated by GAS6 in muscle cells

We hypothesized that GAS6 influences insulin response in insulin-sensitive tissues through binding and activation of one or several of its receptor(s). The expression pattern of GAS6 and TAM receptors across mouse tissues involved in glucose metabolism, including several insulin-sensitive tissues, was therefore investigated. *Gas6* was strongly expressed in eWAT and scWAT but significantly less in BAT, liver and pancreatic islets (**Fig.4A**). *Gas6* mRNA was also highly expressed in oxidative (i.e., soleus) and glycolytic (i.e., gastrocnemius, tibialis anterior, extensor digitorum longus) skeletal muscles (**Fig.4A)**. *Axl* and *MerTK*, but not *Tyro3*, were highly expressed in adipose tissues (**Fig.4B**). *MerTK* was more expressed than *Axl* in liver (**Fig.4C**). TAM receptors were expressed at very low level in mouse islets **(Fig.4D**). Interestingly, *Axl* was the most highly expressed TAM receptor in all types of muscles compared to *MerTK* which was weakly present, while *Tyro3* was undetectable (**Fig.4E**). Since *Gas6* and *Axl* are strongly expressed in skeletal muscle and because this tissue is responsible for ~80% of glucose uptake in

response to insulin in the postprandial state [36], we further investigated a potential implication of GAS6 in the response to insulin in skeletal muscle cells.

To study the action of GAS6 and its receptors on insulin-sensitive cells in vitro, we selected the C2C12 myoblast cell line which can be differentiated into myotubes, respond robustly to insulin [37] and express *Axl* (**Fig.4F**). Since AXL is the TAM family member with the highest affinity for GAS6 [14], we focused our study on this receptor. Recombinant mouse GAS6 was produced and purified in HEK293 Flp-In T-REx cells in the presence of vitamin K to induce its γ-carboxylation (GAS6) or warfarin to produce uncarboxylated GAS6 (uc-GAS6) (**Fig.4G**). Phosphorylation of AXL and its downstream target AKT increased when myotubes were treated with GAS6, but not with uc-GAS6 (**Fig.4H**), confirming that recombinant GAS6 was active, and that γ-carboxylation is necessary for its activity. In addition, GAS6 induces AXL and AKT phosphorylation in a dose-dependent manner with maximal activation between 100 and 200ng/mL (**Fig.4I**).

GAS6 suppresses insulin response in muscle cells

To determine if GAS6 and AXL could impact insulin signaling, C2C12 cells were pre-treated for 8 or 24 hours with GAS6 (200 ng/ml) or vehicle, followed by a 15-minute treatment with insulin. 24-hour long treatment with GAS6 significantly decreases by ~2-fold the phosphorylation of the IR induced by insulin (**Fig.5A-B**). An intermediate, but not significant reduction was observed with the 8-hour GAS6 treatment. The 8-hour GAS6 treatment also reduced AKT phosphorylation on S473, but it reached significance only after cells were pre-treated with GAS6 for 24 hours. (**Fig.5A-B**). Similar results were obtained in L6-GLUT4myc cells, a rat myoblastic cell line

that stably expresses human GLUT4 tagged with a myc epitope (**Fig.S4A**). In this cellular model, 24 hours of GAS6 treatment also reduced insulin-induced translocation of GLUT4 to the plasma membrane (**Fig. S4B**). These results suggest that chronic exposure to GAS6 reduces the capacity of muscle cells to respond to insulin.

AXL interacts with the insulin receptor

It was previously reported that AXL can heterodimerize with other plasma membrane receptors, such as the EGFR, and rewire the signaling pathways elicited by these receptors [38]. In HEK293 cells transfected with AXL-Flag and/or IR-HA expression vectors, IR can be co-immunoprecipitated (co-IP) with AXL (**Fig.5C**). BioID, a proximity biotin labeling assay [39], was used to corroborate these results. HEK293 Flp-In T-REx cells expressing the AXL-BirA*-Flag fusion protein were treated with biotin for 24 hours, biotinylated AXL proximal proteins were pulled-down with streptavidin Sepharose beads and IR detected by Western blot. The results obtained using this approach suggest that endogenous IR does interact with AXL in mammalian cells (**Fig.5D**) and that this interaction is about 4-fold stronger when the cells are stimulated with insulin (**Fig.5E**). In these experiments performed in HEK293 cells and as previously reported [20], we observed that overexpressed AXL-BirA*-Flag was phosphorylated even in the absence of ligand, indicating ligand-independent activation of AXL kinase activity. Taken together, these results suggest that AXL interacts with IR in an insulin-dependent manner.

GAS6 reprograms insulin-dependent signaling pathways in muscle cells

To uncover signaling pathways modulated by GAS6 and impacting insulin signaling, we compared the skeletal muscle (gastrocnemius) transcriptome of *Gas6*$^{+/+}$ and *Gas6*$^{-/-}$ mice. This

analysis revealed that only 17 genes were significantly dysregulated in the absence of GAS6 (*P-adj* < 0.05; **Fig.S5A**). The mRNA encoding for IR (*Insr*) was reduced by ~30% in the muscle of *Gas6*$^{-/-}$ mice, however, this did not translate into a significant change at the protein level (**Fig.S5B**). These results show that GAS6 has a limited effect on muscle gene expression, suggesting that it may influence insulin signaling through post-translational mechanisms.

To understand the molecular impact of GAS6 on insulin-dependent signaling, we performed a quantitative phosphoproteomics screen. C2C12 cells were treated with GAS6 or vehicle for 24 hours, before being stimulated or not with insulin for 15 minutes. Phosphoserine and phosphothreonine containing peptides were enriched using TiO_2 chromatography, labeled with Tandem Mass Tags (TMT) and combined to be analyzed by high-resolution liquid chromatography–tandem MS (LC-MS/MS) to quantify the relative abundance of phosphopeptides modulated by GAS6, insulin or their combination (**Fig.6A**) [40]. The experiment was independently repeated three times, median normalized, and batch effects were corrected. Only the peptides detected and quantified in all the experiments were considered for further analysis. Using this approach, quantitative data were obtained for a total of 1491 unique phosphopeptides, originating from 712 different proteins (**Supplementary Table 3**). We then performed a series of pairwise comparisons and only included peptides that were modulated by at least 1.5-fold between two given conditions with a *P* value ≤ 0.05 (**Fig. 6B** and **Supplementary Table 4**).

Only 54 phosphopeptides were found to be significantly modulated by the 24-hour GAS6 pre-treatment compared to untreated cells (**Fig.6B**). A larger number of phosphorylation sites were up- or down-regulated following the 15 minutes insulin treatment, both in the presence and

absence of GAS6 pretreatment (**Fig.6B-C**). Interestingly, the total number of unique phosphopeptides changed by insulin following GAS6 pretreatment was approximately 6-times higher when compared to insulin alone (549 vs. 107 phosphopeptides; **Fig.6B-C**). However, the overlap between these two groups was limited, with only 24 phosphopeptides upregulated and 16 downregulated by insulin both in the presence and absence of GAS6 (**Fig.6C**), suggesting that GAS6 treatment significantly modifies the insulin-dependent phosphoproteome in C2C12 cells.

A total of 70 phosphosites, contained in 49 different proteins, were upregulated by insulin alone (**Fig.6B; Supplementary Table 5)**. Among those, we identified as expected known downstream targets of the insulin signaling pathway, including IRS1 (S325), AKT1S1 (S210/T273), JUN (S63) or RPS6 (S235/S236/S240/S241). We also identified 37 phosphosites in a total of 32 proteins (**Fig.6B**) whose phosphorylation level was decreased after insulin stimulation. In line with previous phosphoproteomic studies on human muscle cells [41, 42], the phosphorylation of several nuclear proteins, such as MYBBP1A (S1325), ribonucleoprotein NOP58 (S509) and nucleolin (S303), were negatively regulated by insulin.

To determine how GAS6 influences the response to insulin, we next concentrated our analysis on the phosphorylation events differentially affected when comparing insulin with insulin in combination with GAS6 (P-adj <0.05; fold-change ≥ 1.5; **Supplementary Table 6)**. Gene set enrichment analyses were performed with the group of proteins containing these sites to identify specific cellular processes co-regulated by insulin and GAS6. Reactome pathways enrichment analysis showed that proteins whose phosphorylation was decreased in response to insulin in the

presence of GAS6, were mainly associated with RNA metabolism, RhoGTPase signaling, and signal transduction by growth factor receptors (**Fig.7A-B**).

The group of proteins containing phosphorylation sites that are increased by insulin in the presence of GAS6 displayed a very strong enrichment in pathways involving small GTPases of the Rho, Rab, RAC and CDC42 families (**Fig.7C-D**). Importantly, several proteins involved in Rho GTPases signaling contained multiple phosphorylation sites that were up- and down-regulated by insulin in the presence of GAS6 (**Fig.7B and 7D**). While there were no specific changes in phosphorylation of RAC1 and CDC42 GTPases, GAS6 altered the phosphorylation of their GEFs, in response to insulin, respectively DOCK7 and ARHGEF40, as well as their effectors, the kinase of the PAK family (PAK1, PAK2 and PAK4) (**Fig.7C-D**).

The group of proteins containing phosphorylation sites upregulated by insulin in the presence of GAS6 was also enriched in pathways involved in membrane trafficking and vesicle-mediated transport (**Fig.7C-D**). These included SEC31A (S526), a component of the COPII protein complex responsible for vesicle budding from the endoplasmic reticulum (ER) and adaptor-associated protein kinase 1 (AAK1; S635) involved in clathrin-mediated endocytosis. Several proteins in this group have a function in endocytosis and endosomal trafficking which concur with the enrichment of Rab family small GTPases pathways known to control vesicular membrane trafficking to late endosomes (**Fig.7D)**. Altogether, the analysis of this phosphoproteomic study demonstrates that GAS6 significantly modifies the molecular response to insulin. Instead of affecting the canonical insulin signaling pathway, GAS6 appears to regulate proteins involved in small GTPases signaling, endocytosis, vesicle-mediated transport, and membrane trafficking.

AXL signaling increases insulin receptor endocytosis in response to insulin

Analysis of the phosphoproteome uncovered an endosomal trafficking pathway specifically modulated by insulin in the presence of GAS6 and implicating the Rab GTPases, their effectors and other regulators of endocytosis (**Fig.8A**). Endocytosis regulates signaling from tyrosine kinase receptors, including IR [43] and Rab GTPases are known to play a critical role in endosomal trafficking [44]. Formation of late endosomes consists of a transition of Rab5 to Rab7a at their surface. The quantitative proteomic data indicate that Rab7a (S72) itself and TBC1D15 (S205), one of its GAPs, are more phosphorylated following insulin stimulation in the presence of GAS6 (**Fig.8A**). Phosphorylation of Rab7a on S72 was previously shown to facilitate the dynein-driven transport of EGFR, another RTK, toward the perinuclear region [45]. These observations prompted us to investigate whether GAS6- and AXL-elicited signaling could impact insulin receptor (IR) trafficking to late endosomes.

Visualizing IR trafficking in myoblasts or myotubes is challenging due to cell shape, size and autofluorescence. We therefore used HEK293 cells, which express endogenous IR and respond to insulin [46] but do not express AXL [47]. These cells were transfected with mScarlet-tagged Rab7a to visualize late endosomes, and with AXL-Flag or an empty vector, treated with insulin for 15 minutes and the cellular localization of endogenous IR, AXL and Rab7a was assessed by immunofluorescence (**Fig.8B-C**). Stimulation with exogenous GAS6 was not required since AXL is already robustly phosphorylated in the absence of ligand in this experimental model (see **Fig.5D** and [20]). In the absence of AXL and insulin stimulation, IR was detected mostly at the level of the plasma membrane (**Fig.8B-C**). Following a 15-minute treatment with insulin, IR is

partly redistributed from the membrane toward the perinuclear region in Rab7a-positive endosomes (**Fig.8B-D**). In the presence of AXL and in the absence of insulin, the IR exhibits a cellular distribution similar to the one observed in untransfected cells. Strikingly, in the presence of AXL and following insulin stimulation, the intracellular accumulation of IR in the Rab7a-late endosomes was significantly increased (**Fig. 8C-D**). Moreover, the intracellular IR co-localized with AXL, consistent with the observation that these two receptors interact following insulin stimulation. Altogether, these data suggest that AXL signaling potentiates insulin-induced IR trafficking to the late endosomes, potentially explaining the inhibitory effect of GAS6 on insulin signaling in cell culture and insulin sensitivity in vivo.

DISCUSSION

A few studies have investigated the role of GAS6 and AXL in obesity and glucose metabolism using mouse models, leading to conflicting results. It was reported for instance that *Gas6*$^{-/-}$ mice on a mixed genetic background (Swiss:129SV, 50:50) accumulate less WAT compared to *Gas6*$^{+/+}$ mice when fed a high-fat diet [48]. Similarly, treatment with R428 (25mg/kg twice a day), a pharmacological inhibitor of AXL, resulted in significantly reduced weight gain and subcutaneous and gonadal fat mass in C57Bl/6 mice fed a HFD [49]. Interestingly, fed blood glucose was also reduced by the R428 treatment. In contrast, *Axl*$^{-/-}$ mice on a different mixed genetic background (C57Bl/6:129S1, 50:50) fed a HFD displayed no difference in adipose depot mass compared to controls [50]. Importantly, glucose tolerance and insulin sensitivity were not investigated in detail in any of these studies.

Here, we extensively characterize the glucose and metabolic phenotype of *Gas6*$^{-/-}$ mice on two inbred genetic backgrounds. Our data show that in these well-controlled conditions, *Gas6*-deficiency does not impact body weight and adipose tissue mass on normal chow diet or HFHS diet. Importantly, inactivation of *Gas6* does not affect food intake and energy expenditure. However, genetic ablation of GAS6 was associated with reduced blood glucose and improved glucose tolerance and insulin sensitivity. Our data are in line with the previously reported lack of impact of *Axl* inactivation on fat mass on chow or HFD. R428 is a pharmacological inhibitor of AXL which can inhibit other tyrosine kinase receptor at high doses, including IR, EGFR, MerTK and TYRO3. Off-target effects may therefore potentially explain the reported impact of R428 treatment on fat depots in mice.

It was also reported that recombinant GAS6 can increase neonatal pancreatic β-cell proliferation, while inhibiting glucose-stimulated insulin secretion and downregulating the adult β-cell marker *Mafa* [51]. Conversely, R428 dose-dependently increases *MAFA* expression in vitro in β-cells differentiated from human embryonic stem cells (hESC) [52]. Although we did not directly investigate β-cell proliferation in *Gas6*$^{-/-}$ mice, glucose-stimulated insulin secretion was not affected by the absence of GAS6 in adult animals. Altogether, the comprehensive phenotyping of *Gas6*$^{-/-}$ mice presented here reveals that GAS6 negatively impacts glucose handling, mainly by improving whole body insulin sensitivity.

Using two different approaches, co-IP and BioID, we provide evidence of AXL and IR heterodimerization in mammalian cells. AXL has been shown to heterodimerize and/or to crosstalk with other RTK including HER2, EGFR, MET, VEGFR-2 and PDGFRβ [38, 53-55]. In most cases, the heterodimerization of AXL with another RTK was observed in cancer cells overexpressing AXL and found to be critical for tumor cells invasiveness and metastasis [20]. In these instances, AXL appears to potentiate or diversify the signaling pathways emanating from its partner RTK. The IR-AXL crosstalk we describe here is unique since it results in a downregulation of classical IR signaling pathways and an increased trafficking of IR to the late endosomes. Moreover, the IR and AXL interaction appears to be positively regulated by insulin, the IR ligand.

Through a quantitative phosphoproteomics screen, we investigated how a chronic 24h-long GAS6 treatment influences the signaling pathways activated by insulin in muscle cells. In a previous study, we reported the phosphoproteome regulated by a 5-, 10- or 20-minute stimulation

with GAS6 in triple-negative breast cancer (TNBC) [19]. Interestingly, this short stimulation revealed that multiple targets of AXL signaling are shared with IR downstream pathways, including PI3KCA, JNK1/2, ERK1/2 and GSK3α. It was also observed that acute activation of the GAS6/AXL axis influences large phosphoprotein networks involved in actin remodeling, GTPases regulation and RNA transport. Some of those pathways appear to be also co-regulated by GAS6 and insulin in the current study.

Our phosphoproteomic data show that chronic treatment of muscle cells with GAS6 significantly increases phosphorylation of several proteins involved in vesicular trafficking in response to insulin, including proteins of Rab GTPases (e.g., Rab7a S72). Other results presented here revealed that AXL increases the internalization of the IR and in particular its localization in Rab7a-positive endosomes after insulin stimulation. This change in localization corroborate several studies showing a decrease in the levels of IR at the plasma membrane in obese and diabetic conditions [56, 57]. Interestingly, a subclass of IR mutations causing severe insulin resistance and T2D in humans is associated with an abnormal enrichment of the IR in the Rab7a-positive endosomes [58], suggesting that premature or excessive IR endocytosis can contribute to insulin resistance in humans. We thus propose that GAS6 and AXL reprogram insulin signaling pathways and increase the endocytosis of the IR thereby promoting insulin resistance.

In conclusion, our results establish a new role for GAS6 and AXL in the remodeling of insulin signaling in muscle cells and in the development of insulin resistance. This study paves the way for the investigation and development of potential therapeutic approaches using existing pharmacological inhibitors of GAS6/AXL signaling to improve insulin sensitivity.

ACKNOWLEDGEMENTS

We thank Drs M.D. Blostein and P. Carmeliet for providing the *Gas6*$^{-/-}$ strain and Dr A. Robert for generating the pmScarlet-C1-Rab7a plasmid. We also thank the staff of the IRCM Bioinformatics, Proteomics, Microscopy, Molecular Biology and Histology Core Facilities for their technical support. This work was supported by funding from the Fonds de Recherche du Québec Santé (MF), Canada Research Chair program (MF and JFC), Diabetes Canada (MF, OG-3-21-5599-MF), the Canadian Institutes of Health Research (MF, PJT-159534; JFC, PJT-178083), the Fonds de Recherche du Québec Santé (MF) and the Cardiometabolic health Diabetes Obesity (CMDO) Network (MF). CS received scholarships from IRCM and the Fonds de Recherche du Québec Santé. AG received scholarships from IRCM, the Montreal Diabetes Research Center and Diabète Québec. JL received a fellowship from Diabetes Canada.

AUTHOR CONTRIBUTIONS

MF and JL conceived, designed the project, and supervised CS and AG. CS, AG, JL, DF, JB and MF collected and analyzed data. JFC provided unique reagents and critical advice for experiments. CS and MF wrote the manuscript with suggestion from the other authors.

Disclosure Summary: The authors have nothing to disclose.

REFERENCES

1. Haeusler, R.A., et al., *Biochemical and cellular properties of insulin receptor signalling.* Nat Rev Mol Cell Biol, 2018. **19**(1): p. 31-44.
2. Boucher, J., et al., *Insulin receptor signaling in normal and insulin-resistant states.* Cold Spring Harb Perspect Biol, 2014. **6**(1).
3. Cusi, K., et al., *Insulin resistance differentially affects the PI 3-kinase- and MAP kinase-mediated signaling in human muscle.* J Clin Invest, 2000. **105**(3): p. 311-20.
4. Krook, A., et al., *Characterization of signal transduction and glucose transport in skeletal muscle from type 2 diabetic patients.* Diabetes, 2000. **49**(2): p. 284-92.
5. Bouzakri, K., et al., *Reduced activation of phosphatidylinositol-3 kinase and increased serine 636 phosphorylation of insulin receptor substrate-1 in primary culture of skeletal muscle cells from patients with type 2 diabetes.* Diabetes, 2003. **52**(6): p. 1319-25.
6. Schneider, C., et al., *Genes specifically expressed at growth arrest of mammalian cells.* Cell, 1988. **54**(6): p. 787-93.
7. Gely-Pernot, A., et al., *An endogenous vitamin K-dependent mechanism regulates cell proliferation in the brain subventricular stem cell niche.* Stem Cells, 2012. **30**(4): p. 719-31.
8. Hasanbasic, I., et al., *The role of gamma-carboxylation in the anti-apoptotic function of gas6.* J Thromb Haemost, 2005. **3**(12): p. 2790-7.
9. Rajotte, I., et al., *Gas6-mediated signaling is dependent on the engagement of its gamma-carboxyglutamic acid domain with phosphatidylserine.* Biochem Biophys Res Commun, 2008. **376**(1): p. 70-3.
10. Varnum, B.C., et al., *Axl receptor tyrosine kinase stimulated by the vitamin K-dependent protein encoded by growth-arrest-specific gene 6.* Nature, 1995. **373**(6515): p. 623-6.
11. Burstyn-Cohen, T., et al., *Lack of protein S in mice causes embryonic lethal coagulopathy and vascular dysgenesis.* J Clin Invest, 2009. **119**(10): p. 2942-53.
12. Angelillo-Scherrer, A., et al., *Deficiency or inhibition of Gas6 causes platelet dysfunction and protects mice against thrombosis.* Nat Med, 2001. **7**(2): p. 215-21.
13. Lew, E.D., et al., *Differential TAM receptor-ligand-phospholipid interactions delimit differential TAM bioactivities.* Elife, 2014. **3**.
14. Tsou, W.I., et al., *Receptor tyrosine kinases, TYRO3, AXL, and MER, demonstrate distinct patterns and complex regulation of ligand-induced activation.* J Biol Chem, 2014. **289**(37): p. 25750-63.
15. Lu, Q., et al., *Tyro-3 family receptors are essential regulators of mammalian spermatogenesis.* Nature, 1999. **398**(6729): p. 723-8.

16. Lemke, G. and T. Burstyn-Cohen, *TAM receptors and the clearance of apoptotic cells.* Ann N Y Acad Sci, 2010. **1209**: p. 23-9.

17. Rothlin, C.V., et al., *TAM receptors are pleiotropic inhibitors of the innate immune response.* Cell, 2007. **131**(6): p. 1124-36.

18. Angelillo-Scherrer, A., et al., *Role of Gas6 receptors in platelet signaling during thrombus stabilization and implications for antithrombotic therapy.* J Clin Invest, 2005. **115**(2): p. 237-46.

19. Abu-Thuraia, A., et al., *AXL confers cell migration and invasion by hijacking a PEAK1-regulated focal adhesion protein network.* Nat Commun, 2020. **11**(1): p. 3586.

20. Goyette, M.A., et al., *The Receptor Tyrosine Kinase AXL Is Required at Multiple Steps of the Metastatic Cascade during HER2-Positive Breast Cancer Progression.* Cell Rep, 2018. **23**(5): p. 1476-1490.

21. Burstyn-Cohen, T., et al., *Genetic dissection of TAM receptor-ligand interaction in retinal pigment epithelial cell phagocytosis.* Neuron, 2012. **76**(6): p. 1123-32.

22. Kuo, F.C., et al., *The levels of plasma growth arrest-specific protein 6 is associated with insulin sensitivity and inflammation in women.* Diabetes Res Clin Pract, 2014. **103**(2): p. 304-9.

23. Hung, Y.J., et al., *Plasma protein growth arrest-specific 6 levels are associated with altered glucose tolerance, inflammation, and endothelial dysfunction.* Diabetes Care, 2010. **33**(8): p. 1840-4.

24. Hsiao, F.C., et al., *Circulating growth arrest-specific 6 protein is associated with adiposity, systemic inflammation, and insulin resistance among overweight and obese adolescents.* J Clin Endocrinol Metab, 2013. **98**(2): p. E267-74.

25. Wheeler, E., et al., *Impact of common genetic determinants of Hemoglobin A1c on type 2 diabetes risk and diagnosis in ancestrally diverse populations: A transethnic genome-wide meta-analysis.* PLoS Med, 2017. **14**(9): p. e1002383.

26. Nag, A., et al., *Human genetics uncovers MAP3K15 as an obesity-independent therapeutic target for diabetes.* Sci Adv, 2022. **8**(46): p. eadd5430.

27. Al Rifai, O., et al., *Proprotein convertase furin regulates osteocalcin and bone endocrine function.* J Clin Invest, 2017. **127**(11): p. 4104-4117.

28. Berglund, E.D., et al., *Glucose metabolism in vivo in four commonly used inbred mouse strains.* Diabetes, 2008. **57**(7): p. 1790-9.

29. Kim, D.H., et al., *Increased adipose tissue hypoxia and capacity for angiogenesis and inflammation in young diet-sensitive C57 mice compared with diet-resistant FVB mice.* Int J Obes (Lond), 2013. **37**(6): p. 853-60.

30. Xu, H., et al., *Chronic inflammation in fat plays a crucial role in the development of obesity-related insulin resistance.* J Clin Invest, 2003. **112**(12): p. 1821-30.

31. Carrera Silva, E.A., et al., *T cell-derived protein S engages TAM receptor signaling in dendritic cells to control the magnitude of the immune response.* Immunity, 2013. **39**(1): p. 160-70.

32. Lemke, G. and C.V. Rothlin, *Immunobiology of the TAM receptors.* Nat Rev Immunol, 2008. **8**(5): p. 327-36.

33. Allan, C.M., et al., *Two hepatic enhancers, HCR.1 and HCR.2, coordinate the liver expression of the entire human apolipoprotein E/C-I/C-IV/C-II gene cluster.* J Biol Chem, 1997. **272**(46): p. 29113-9.

34. Lacombe, J., et al., *VKOR paralog VKORC1L1 supports vitamin K-dependent protein carboxylation in vivo.* JCI Insight, 2018. **3**(1).

35. Alquier, T. and V. Poitout, *Considerations and guidelines for mouse metabolic phenotyping in diabetes research.* Diabetologia, 2018. **61**(3): p. 526-538.

36. Thiebaud, D., et al., *The effect of graded doses of insulin on total glucose uptake, glucose oxidation, and glucose storage in man.* Diabetes, 1982. **31**(11): p. 957-63.

37. Mangnall, D., et al., *Insulin-stimulated glucose uptake in C2C12 myoblasts.* Biochem Soc Trans, 1993. **21**(4): p. 438S.

38. Meyer, A.S., et al., *The receptor AXL diversifies EGFR signaling and limits the response to EGFR-targeted inhibitors in triple-negative breast cancer cells.* Sci Signal, 2013. **6**(287): p. ra66.

39. Roux, K.J., et al., *A promiscuous biotin ligase fusion protein identifies proximal and interacting proteins in mammalian cells.* J Cell Biol, 2012. **196**(6): p. 801-10.

40. Navarrete-Perea, J., et al., *Streamlined Tandem Mass Tag (SL-TMT) Protocol: An Efficient Strategy for Quantitative (Phospho)proteome Profiling Using Tandem Mass Tag-Synchronous Precursor Selection-MS3.* J Proteome Res, 2018. **17**(6): p. 2226-2236.

41. Batista, T.M., et al., *A Cell-Autonomous Signature of Dysregulated Protein Phosphorylation Underlies Muscle Insulin Resistance in Type 2 Diabetes.* Cell Metab, 2020. **32**(5): p. 844-859 e5.

42. Haider, N., et al., *Signaling defects associated with insulin resistance in nondiabetic and diabetic individuals and modification by sex.* J Clin Invest, 2021. **131**(21).

43. Goh, L.K. and A. Sorkin, *Endocytosis of receptor tyrosine kinases.* Cold Spring Harb Perspect Biol, 2013. **5**(5): p. a017459.

44. Wandinger-Ness, A. and M. Zerial, *Rab proteins and the compartmentalization of the endosomal system.* Cold Spring Harb Perspect Biol, 2014. **6**(11): p. a022616.

45. Hanafusa, H., et al., *LRRK1 phosphorylation of Rab7 at S72 links trafficking of EGFR-containing endosomes to its effector RILP.* J Cell Sci, 2019. **132**(11).

46. Wharton, J., et al., *Dissociation of insulin receptor expression and signaling from caveolin-1 expression.* J Biol Chem, 2005. **280**(14): p. 13483-6.

47. Zdzalik-Bielecka, D., et al., *The GAS6-AXL signaling pathway triggers actin remodeling that drives membrane ruffling, macropinocytosis, and cancer-cell invasion.* Proc Natl Acad Sci U S A, 2021. **118**(28).

48. Maquoi, E., et al., *Role of Gas-6 in adipogenesis and nutritionally induced adipose tissue development in mice.* Arterioscler Thromb Vasc Biol, 2005. **25**(5): p. 1002-7.

49. Lijnen, H.R., et al., *Growth arrest-specific protein 6 receptor antagonism impairs adipocyte differentiation and adipose tissue development in mice.* J Pharmacol Exp Ther, 2011. **337**(2): p. 457-64.

50. Scroyen, I., et al., *Axl deficiency does not affect adipogenesis or adipose tissue development.* Obesity (Silver Spring), 2012. **20**(6): p. 1168-73.

51. Haase, T.N., et al., *Growth arrest specific protein (GAS) 6: a role in the regulation of proliferation and functional capacity of the perinatal rat beta cell.* Diabetologia, 2013. **56**(4): p. 763-73.

52. Rezania, A., et al., *Reversal of diabetes with insulin-producing cells derived in vitro from human pluripotent stem cells.* Nat Biotechnol, 2014. **32**(11): p. 1121-33.

53. Adam-Artigues, A., et al., *Targeting HER2-AXL heterodimerization to overcome resistance to HER2 blockade in breast cancer.* Sci Adv, 2022. **8**(20): p. eabk2746.

54. Ruan, G.X. and A. Kazlauskas, *Axl is essential for VEGF-A-dependent activation of PI3K/Akt.* EMBO J, 2012. **31**(7): p. 1692-703.

55. Salian-Mehta, S., et al., *AXL and MET crosstalk to promote gonadotropin releasing hormone (GnRH) neuronal cell migration and survival.* Mol Cell Endocrinol, 2013. **374**(1-2): p. 92-100.

56. Choi, E., et al., *Mitotic regulators and the SHP2-MAPK pathway promote IR endocytosis and feedback regulation of insulin signaling.* Nat Commun, 2019. **10**(1): p. 1473.

57. Soll, A.H., et al., *Insulin binding to liver plasm membranes in the obese hyperglycemic (ob/ob) mouse. Demonstration of a decreased number of functionally normal receptors.* J Biol Chem, 1975. **250**(12): p. 4702-7.

58. Hall, C., et al., *Insulin receptor endocytosis in the pathophysiology of insulin resistance.* Exp Mol Med, 2020. **52**(6): p. 911-920.

FIGURE LEGENDS

Figure 1. GAS6 deficiency improves glucose tolerance and insulin sensitivity in FVB/N and C57BL/6J mice under chow diet. Metabolic parameters of 3-month-old *Gas6*$^{+/+}$ and *Gas6*$^{-/-}$ FVB/N (blue) and C57BL/6J (red) male mice. **(A-B)** Fed and fasting (5h or 16h) blood glucose levels (n=5-10). **(C-D)** Intraperitoneal glucose tolerance Test (IPGTT) and area under the curve (AUC) (n=11-25). Mice were fasted for 16 hours and injected i.p. with 2g/kg of glucose. **(E-F)** For insulin tolerance test (ITT), mice were fasted for 5 hours and injected i.p. with 0.6 U/kg of insulin (n=14-25). Results are expressed as a percentage of basal glycemia and AUC. **(G-H)** Glucose stimulated insulin secretion (GSIS) test and AUC in mice injected i.p. with 3g/kg of glucose after 16 hours of fasting (n=7-9). Results represent mean ± SEM, **P* < 0.05, ***P* < 0.01, ****P* < 0.001 by unpaired, 2-tailed Student's *t* test **(A-B** and for AUC in **C-H)**, or by two-way ANOVA for repeated measurements with Bonferroni's post tests **(C-H)**.

Figure 2. GAS6 deficiency protects from High-Fat/High-Sucrose diet-induced insulin resistance independently of body weight. **(A)** Body weight, percentage of total **(B)** fat and **(C)** lean mass over body weight and **(D)** epididymal and **(E)** subcutaneous fat pad weight of *Gas6*$^{+/+}$ and *Gas6*$^{-/-}$ C57BL/6J mice fed a chow diet (Chow) or a High-Fat/High-Sucrose diet (HFHS) for 12 weeks (n=8-12). **(F)** Six hours fasting blood glucose. **(G)** IPGTT results and AUC (n=8-12). Mice were fasted for 5 hours and injected i.p. with 1g/kg glucose. **(H)** ITT in mice after a 5h-fast and injected i.p. with 0.75U/kg of insulin (n=7-11). Results are expressed as a percentage of basal glycemia and as AUC. **(I)** GSIS test in mice fasted for 16 hours and injected i.p with 3g/kg glucose (n=10-11) and AUC. Results represent mean ± SEM. **P* < 0.05, ***P* < 0.01, ****P* < 0.001, by two-way ANOVA for repeated measurements with Bonferroni's post tests **(A** and **G-I)**,

by one-way ANOVA with by Bonferroni's post tests **(B-F** and AUC for **G)** or by unpaired, 2-tailed Student's *t* test **(**AUC in **H-I)**.

Figure 3. Increasing GAS6 circulating levels reduces insulin sensitivity. (A) Schematic representation of the construct used to generate *ApoE-Gas6*^{Tg} mice. *Gas6-Myc-6xHis* was cloned in the pLIV.7 vector containing exon 1 and 2, liver-specific regulatory sequences and 5′ and 3′ flanking sequences of the human *APOE* gene. **(B)** *Gas6* gene expression in tissues from WT and *ApoE-Gas6*^{Tg} mice was assessed by quantitative PCR (qPCR) and normalized to *Actb* (*n* = 3-5). **(C)** GAS6 serum levels in WT and *ApoE-Gas6*^{Tg} mice were measured by ELISA (n=6-10). **(D)** Body weight of WT and *ApoE-Gas6*^{Tg} mice at 3 and 6 months of age (n=7-11). **(E** and **G)** Fed and fasting (5h or 16h) blood glucose levels in WT and *ApoE-Gas6*^{Tg} mice at 3 and 6 months of age (n=12-24). **(F** and **H)** ITT results at 3 and 6 months of age; mice were fasted for 5 hours and injected i.p. with 0.75U/kg of insulin (n=10-19). Results are expressed as a percentage of basal glycemia and as AUC. Results represent mean ± SEM, $*P < 0.05$, $**P < 0.01$, $***P < 0.001$ by unpaired, 2-tailed Student's *t* test **(B-E and G** and AUC in **F** and **H)**, or by two-way ANOVA for repeated measurements with Bonferroni's post tests **(F and H)**.

Figure 4. GAS6 activates AXL in muscle cells. (A) *Gas6* and **(B-E)** *Axl*, *Mertk* and *Tyro3* (TAM receptors) expression in WT (C57BL/6J) mouse tissues measured by quantitative PCR (qPCR) (n=3). eWAT: epididymal white adipose tissue; scWAT: subcutaneous white adipose tissue; BAT: brown adipose tissue; Gastroc: gastrocnemius; EDL: extensor digitorum longus; TA: tibialis anterior. Results are represented as copy number normalized to *S16*. **(F)** TAM receptors expression in C2C12 cells was measured by qPCR (n=4). Results are represented as copy number normalized to *S16*. **(G)** Recombinant GAS6 carboxylation and expression at

different steps of GAS6 purification, tested using α-Gla antibodies by Western blot analysis. α-Myc was used to identify GAS6-Myc-6×His protein. **(H)** Phosphorylation of AXL (Y702) and AKT (S473) in C2C12 myotubes treated with uncarboxylated (uc-GAS6) or carboxylated GAS6 (GAS6: 100 and 200 ng/mL) for 15 minutes. Total AXL and total AKT were used as loading controls. **(I)** Dose-response of AXL and AKT phosphorylation in C2C12 cells treated with GAS6 for 15 minutes. Results represent mean ± SEM, $*P < 0.05$, $**P < 0.01$, $***P < 0.001$ by one-way ANOVA with Bonferroni's post test **(B-E)**. Western blot are representative experiments of at least 3 independent experiments.

Figure 5. GAS6 suppresses insulin signaling in C2C12 and AXL interacts with the insulin receptor. (A) Phosphorylation of the insulin receptor (IR-Y1150/1151) and AKT (S473) assessed by Western blot in C2C12 cells treated with GAS6 (200 ng/ml) for 8h or 24h followed by insulin stimulation (100 nM) for 15 minutes. Total IR and total AKT were used as loading controls. **(B)** Quantification of phosphorylation levels of IR and AKT normalized over the amount of total protein (n=3). **(C)** Co-immunoprecipitation (IP) in HEK293 transfected with AXL-BirA*-Flag and IR-HA plasmids. **(D)** Proximity-dependent biotinylation (BioID) assay performed in HEK293 Flp-In T-REx cells expressing AXL-BirA*-Flag. **(E)** Quantification of endogenous IR signal detected by streptavidin pulldown and normalized over the biotin only condition. Results represent mean ± SEM. $*P < 0.05$, by one-way ANOVA followed by Bonferroni's post test (n=3). Western blot are representative experiments of 3 independent experiments.

Figure 6. GAS6 reprograms the insulin-dependent phosphoproteome in muscle cells. (A) Schematic representation of the experimental design, including phospho-enrichment, TMT labelling and LC-MS/MS analysis of C2C12 treated for 24 hours with GAS6 (200ng/ml) followed by 15 minutes of insulin stimulation (100nM). The phosphosproteomic screen was performed on samples from 3 independent experiments. **(B)** Volcanoplots of phosphosites significantly changed ($P < 0.05$) between the different treatments. Fold change is represented as and log2 Fold change ≥ 0.5 (red plots) or ≤ -0.5 (blue plots). **(C)** Venn diagram of phosphosites upregulated and downregulated by insulin or GAS6 + insulin treatments in comparison to untreated condition (i.e, no insulin).

Figure 7. GAS6 rewires insulin signaling pathways in muscle cells. (A) Reactome pathway analysis of proteins with decreased phosphorylation when C2C12 cells were treated with GAS6 in combination with insulin compared to insulin alone, generated by Gene Set Enrichment Analysis (FDR q-value < 0.05). The number of proteins associated to each pathway is indicated next to each bar graphs. **(B)** Protein-protein interaction network analysis of proteins with decreased phosphorylation when treated with GAS6 and insulin compared to insulin alone, generated using STRING and Cytoscape. **(C)** Results of GSEA Reactome pathway analysis of proteins with increased phosphorylation when treated with GAS6 in combination with insulin compared to insulin alone (FDR q-value < 0.05). The number of proteins associated to each pathway is indicated next to each bar graphs. **(D)** Network layout of protein-protein interaction of proteins with increased phosphorylation when C2C12 cells were treated with GAS6 in combination with insulin compared to insulin alone, generated using STRING and Cytoscape.

Figure 8. AXL increases insulin receptor endocytosis in response to insulin. (A) Schematic of the endocytosis pathway involving Rab proteins specifically affected by insulin and GAS6 co-treatment. Upregulated and downregulated phosphosites by insulin in combination with GAS6 are represented in red and blue respectively. **(B)** Representative confocal microscopy images of HEK293 cells transfected with Rab7-mScarlet and AXL-Flag or empty vector, and treated or not with 100 nM insulin for 15 minutes. Cells were stained for AXL-Flag (Alexa Fluor 633-magenta) and endogenous IR (Alexa-Fluor 488/green). DAPI was used to stain nuclei. Scale bar, 10 µm. **(C)** Quantification of IR fluorescence signal from the nucleus to the plasma membrane in the different indicated conditions. **(D)** IR and Rab7 fluorescence signal in the respective conditions. Results represent mean ± SEM (n=30 cells per condition, from 3 independent experiments).

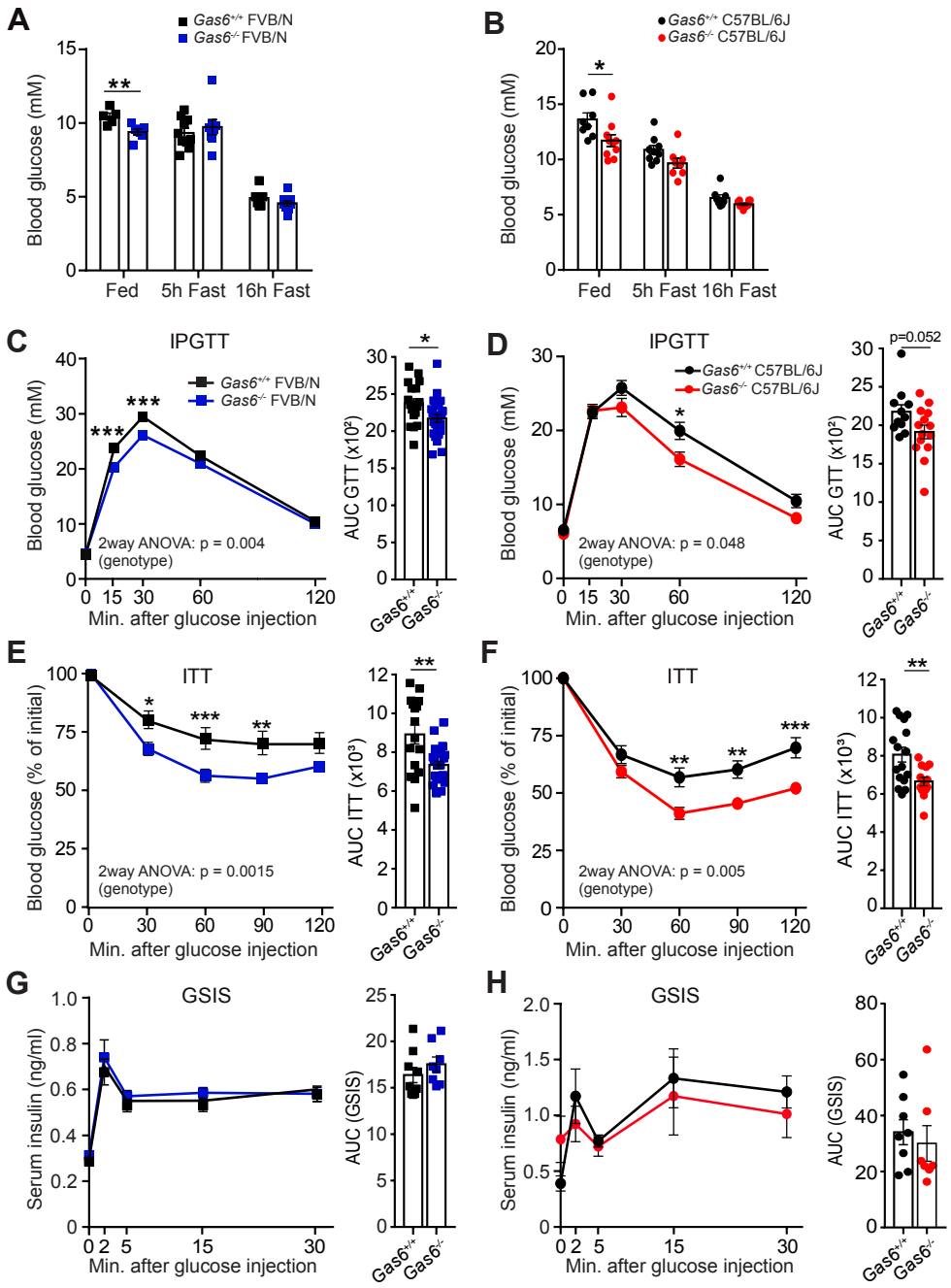
A
Gas6+/+ FVB/N
Gas6-/- FVB/N
Blood glucose (mM)
Fed
5h Fast
16h Fast
B
Gas6+/+ C57BL/6J
Gas6-/- C57BL/6J
C
IPGTT
2way ANOVA: p = 0.004 (genotype)
Min. after glucose injection
AUC GTT (x10²)
D
IPGTT
2way ANOVA: p = 0.048 (genotype)
p=0.052
E
ITT
2way ANOVA: p = 0.0015 (genotype)
Blood glucose (% of initial)
AUC ITT (x10³)
F
ITT
2way ANOVA: p = 0.005 (genotype)
G
GSIS
Serum insulin (ng/ml)
AUC (GSIS)
H
GSIS

Figure 1

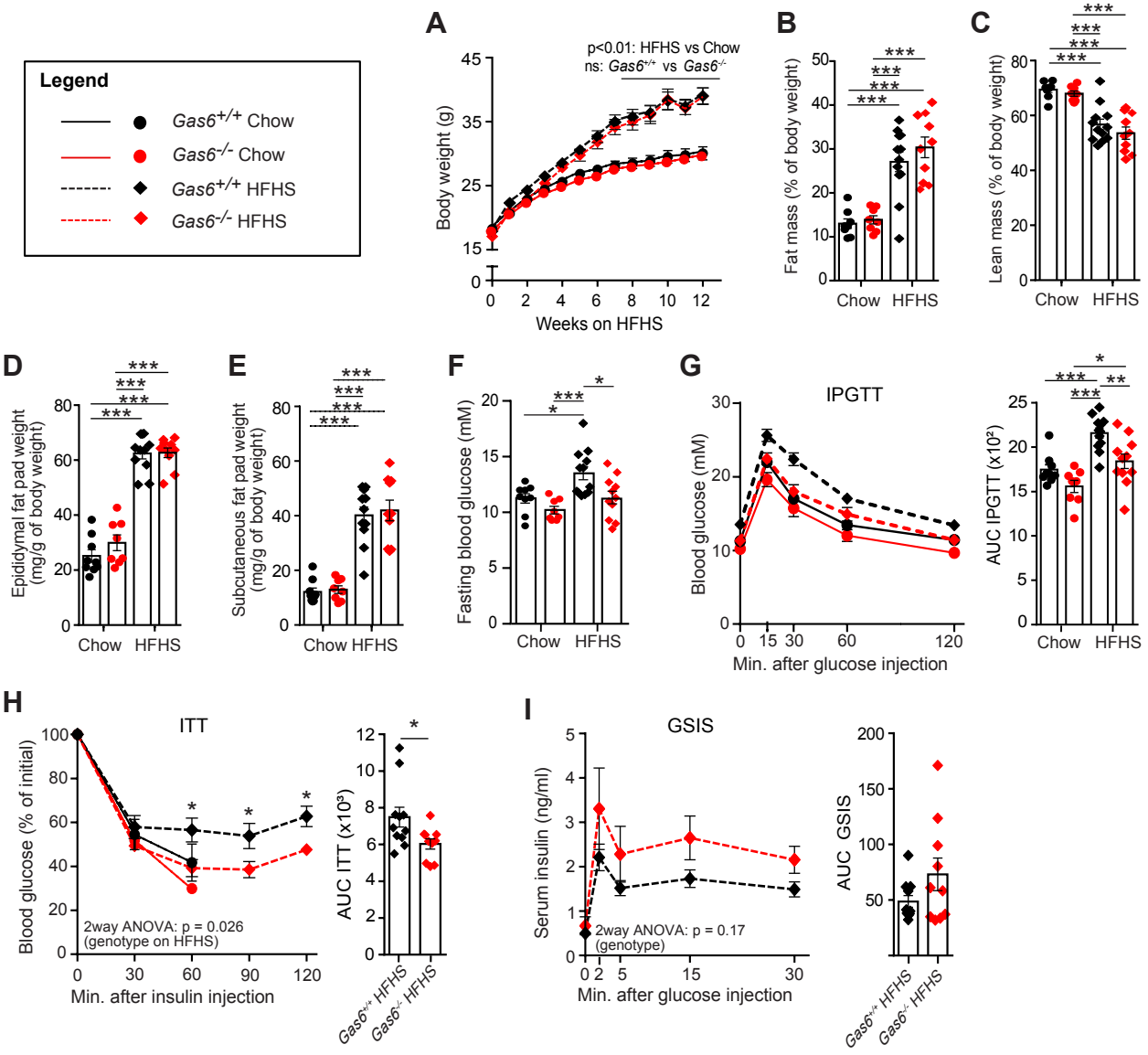
Legend
Gas6+/+ Chow
Gas6-/- Chow
Gas6+/+ HFHS
Gas6-/- HFHS
A
p<0.01: HFHS vs Chow
ns: Gas6+/+ vs Gas6-/-
Body weight (g)
Weeks on HFHS
B
Fat mass (% of body weight)
Chow
HFHS
C
Lean mass (% of body weight)
D
Epididymal fat pad weight (mg/g of body weight)
E
Subcutaneous fat pad weight (mg/g of body weight)
F
Fasting blood glucose (mM)
G
IPGTT
Blood glucose (mM)
Min. after glucose injection
AUC IPGTT (x10²)
H
ITT
Blood glucose (% of initial)
2way ANOVA: p = 0.026 (genotype on HFHS)
Min. after insulin injection
AUC ITT (x10³)
Gas6+/+ HFHS
Gas6-/- HFHS
I
GSIS
Serum insulin (ng/ml)
2way ANOVA: p = 0.17 (genotype)
Min. after glucose injection
AUC GSIS

Figure 2

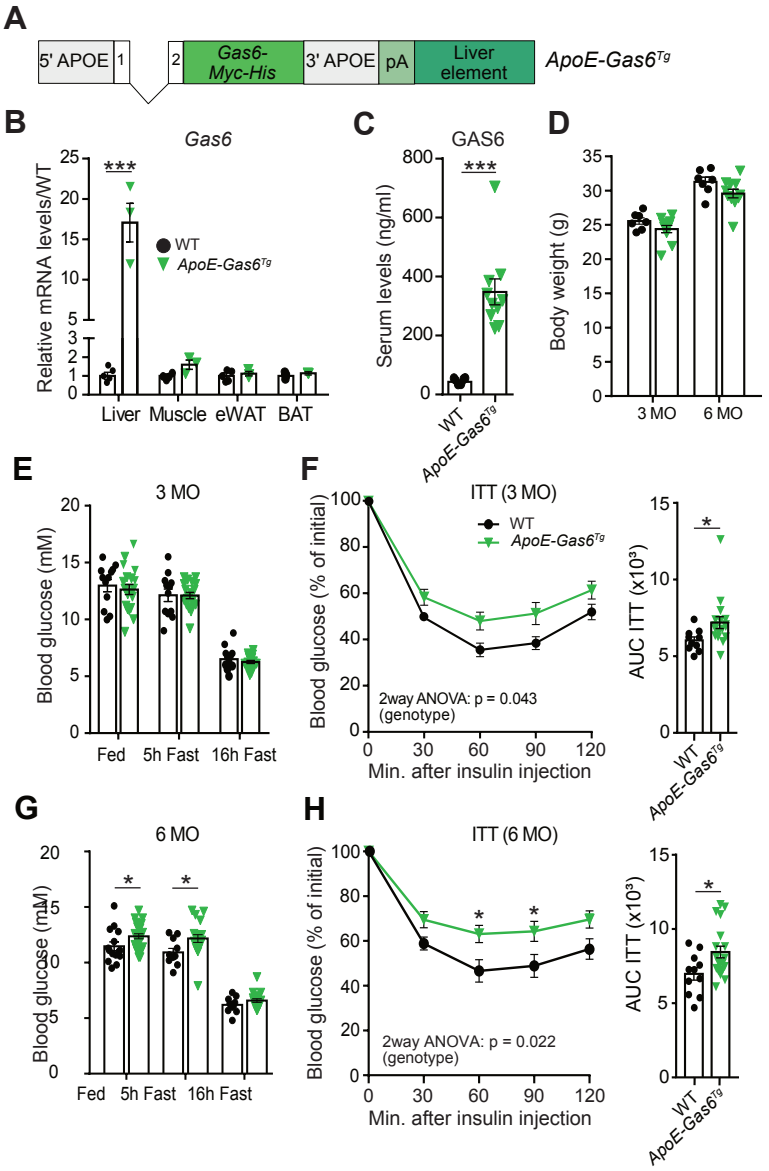
A
5' APOE
1
2
Gas6-Myc-His
3' APOE
pA
Liver element
ApoE-Gas6Tg
B
Gas6
Relative mRNA levels/WT
***
WT
ApoE-Gas6Tg
Liver
Muscle
eWAT
BAT
C
GAS6
Serum levels (ng/ml)
***
WT
ApoE-Gas6Tg
D
Body weight (g)
3 MO
6 MO
E
3 MO
Blood glucose (mM)
Fed
5h Fast
16h Fast
F
ITT (3 MO)
Blood glucose (% of initial)
WT
ApoE-Gas6Tg
2way ANOVA: p = 0.043
(genotype)
Min. after insulin injection
AUC ITT (x10³)
*
WT
ApoE-Gas6Tg
G
6 MO
Blood glucose (mM)
*
*
Fed
5h Fast
16h Fast
H
ITT (6 MO)
Blood glucose (% of initial)
*
*
2way ANOVA: p = 0.022
(genotype)
Min. after insulin injection
AUC ITT (x10³)
*
WT
ApoE-Gas6Tg

Figure 3

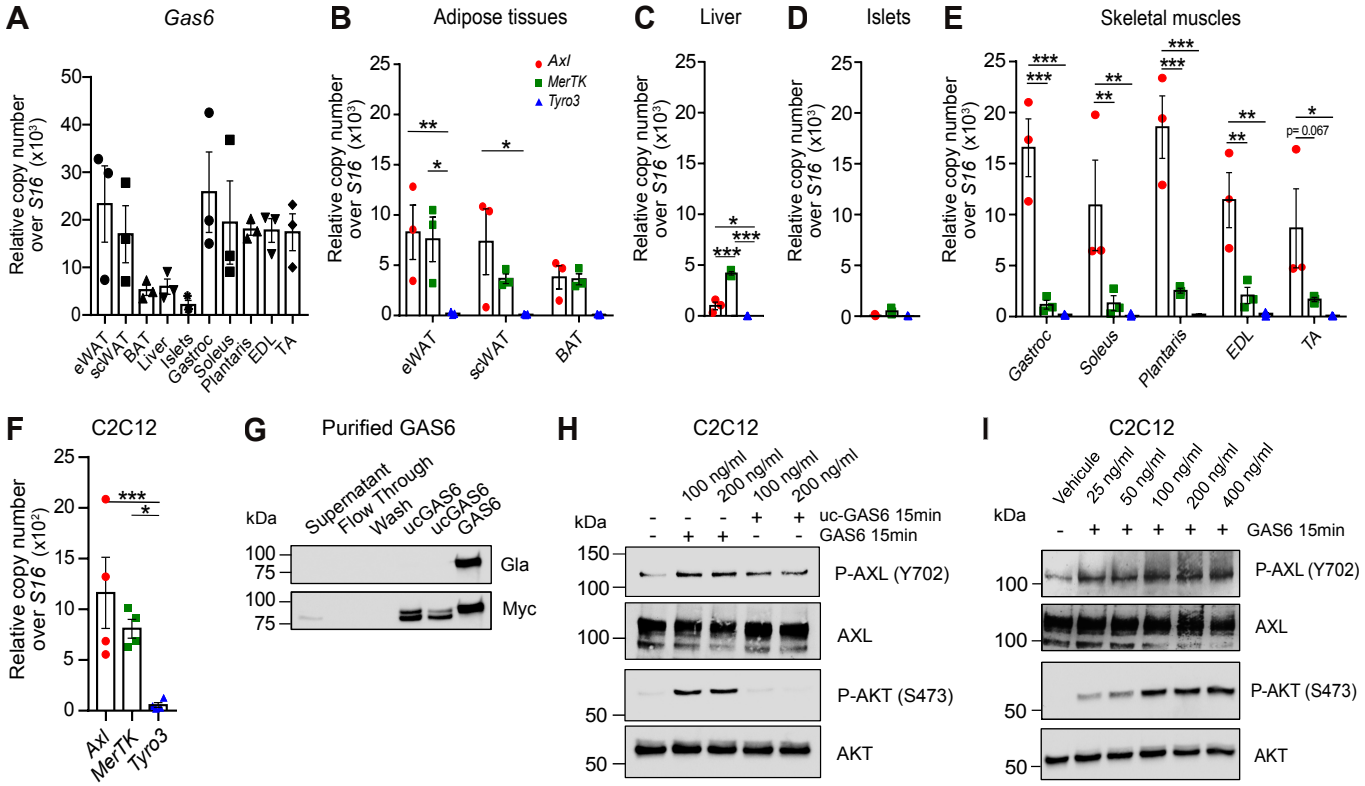
A
Gas6
Relative copy number over S16 (x10³)
eWAT
scWAT
BAT
Liver
Islets
Gastroc
Soleus
Plantaris
EDL
TA
B
Adipose tissues
Axl
MerTK
Tyro3
C
Liver
D
Islets
E
Skeletal muscles
p= 0.067
F
C2C12
Relative copy number over S16 (x10²)
G
Purified GAS6
Supernatant
Flow Through
Wash
ucGAS6
ucGAS6
GAS6
kDa
Gla
Myc
H
C2C12
100 ng/ml
200 ng/ml
uc-GAS6 15min
GAS6 15min
P-AXL (Y702)
AXL
P-AKT (S473)
AKT
I
C2C12
Vehicule
25 ng/ml
50 ng/ml
100 ng/ml
200 ng/ml
400 ng/ml
GAS6 15min

Figure 4

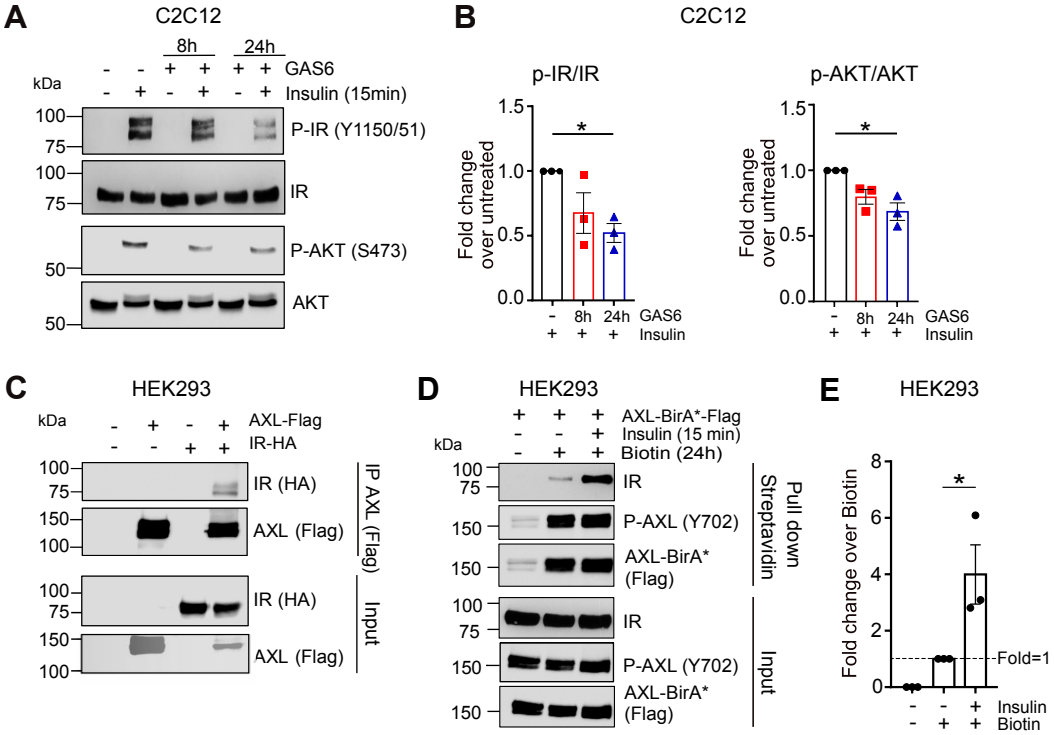
A
C2C12
8h
24h
GAS6
Insulin (15min)
kDa
P-IR (Y1150/51)
IR
P-AKT (S473)
AKT
B
C2C12
p-IR/IR
p-AKT/AKT
Fold change over untreated
GAS6
Insulin
C
HEK293
AXL-Flag
IR-HA
IR (HA)
AXL (Flag)
IP AXL (Flag)
Input
D
HEK293
AXL-BirA*-Flag
Insulin (15 min)
Biotin (24h)
IR
P-AXL (Y702)
AXL-BirA* (Flag)
Pull down Streptavidin
Input
E
HEK293
Fold change over Biotin
Fold=1
Insulin
Biotin

Figure 5

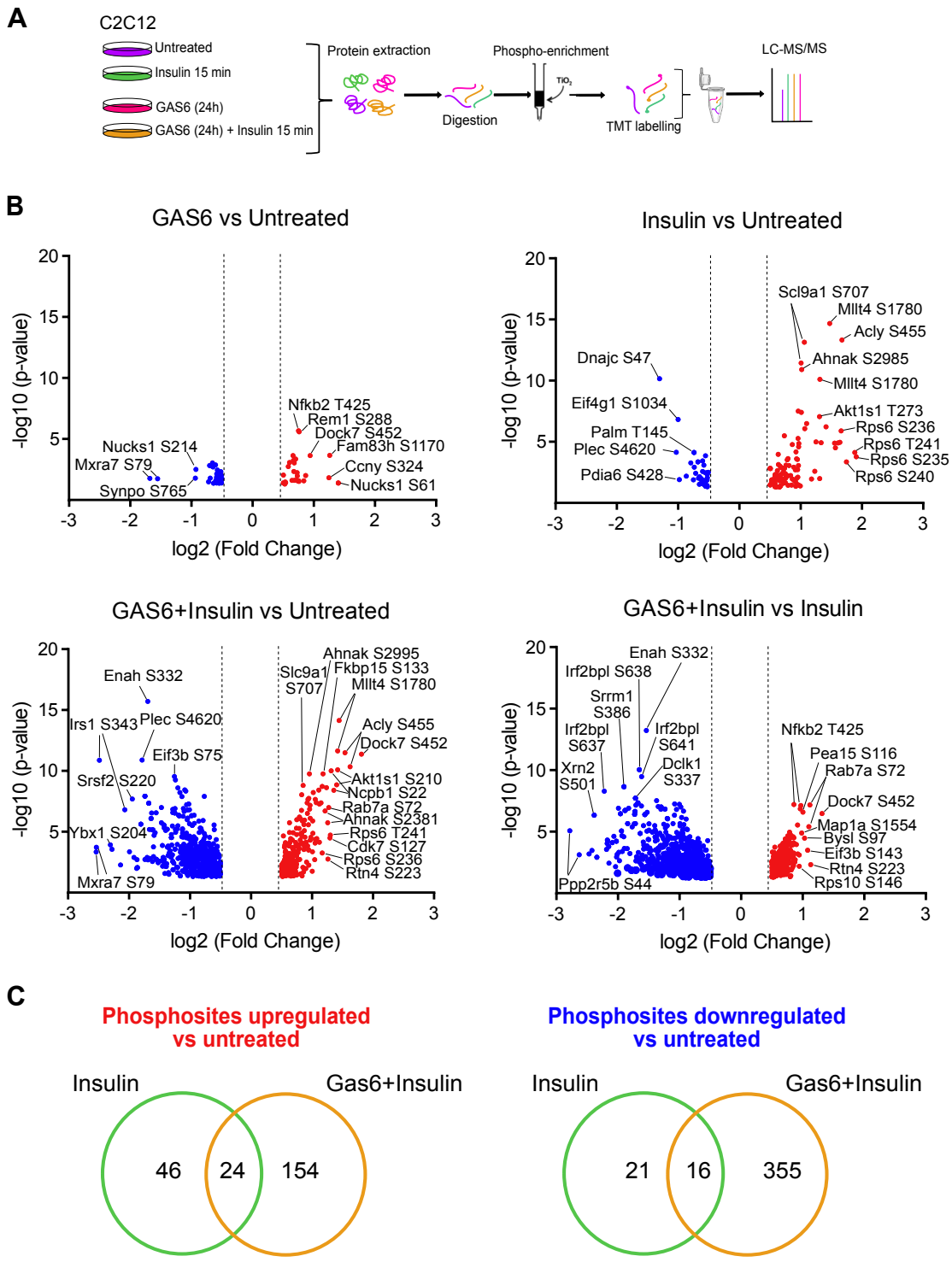
A
C2C12
Untreated
Insulin 15 min
GAS6 (24h)
GAS6 (24h) + Insulin 15 min
Protein extraction
Digestion
Phospho-enrichment
TiO2
TMT labelling
LC-MS/MS
B
GAS6 vs Untreated
Nucks1 S214
Mxra7 S79
Synpo S765
Nfkb2 T425
Rem1 S288
Dock7 S452
Fam83h S1170
Ccny S324
Nucks1 S61
Insulin vs Untreated
Dnajc S47
Eif4g1 S1034
Palm T145
Plec S4620
Pdia6 S428
Scl9a1 S707
Mllt4 S1780
Acly S455
Ahnak S2985
Mllt4 S1780
Akt1s1 T273
Rps6 S236
Rps6 T241
Rps6 S235
Rps6 S240
GAS6+Insulin vs Untreated
Enah S332
Irs1 S343
Plec S4620
Eif3b S75
Srsf2 S220
Ybx1 S204
Mxra7 S79
Ahnak S2995
Slc9a1 S707
Fkbp15 S133
Mllt4 S1780
Acly S455
Dock7 S452
Akt1s1 S210
Ncpb1 S22
Rab7a S72
Ahnak S2381
Rps6 T241
Cdk7 S127
Rps6 S236
Rtn4 S223
GAS6+Insulin vs Insulin
Enah S332
Irf2bpl S638
Srrm1 S386
Irf2bpl S637
Irf2bpl S641
Xrn2 S501
Dclk1 S337
Ppp2r5b S44
Nfkb2 T425
Pea15 S116
Rab7a S72
Dock7 S452
Map1a S1554
Bysl S97
Eif3b S143
Rtn4 S223
Rps10 S146
-log10 (p-value)
log2 (Fold Change)
C
Phosphosites upregulated vs untreated
Insulin
Gas6+Insulin
46
24
154
Phosphosites downregulated vs untreated
Insulin
Gas6+Insulin
21
16
355

Figure 6

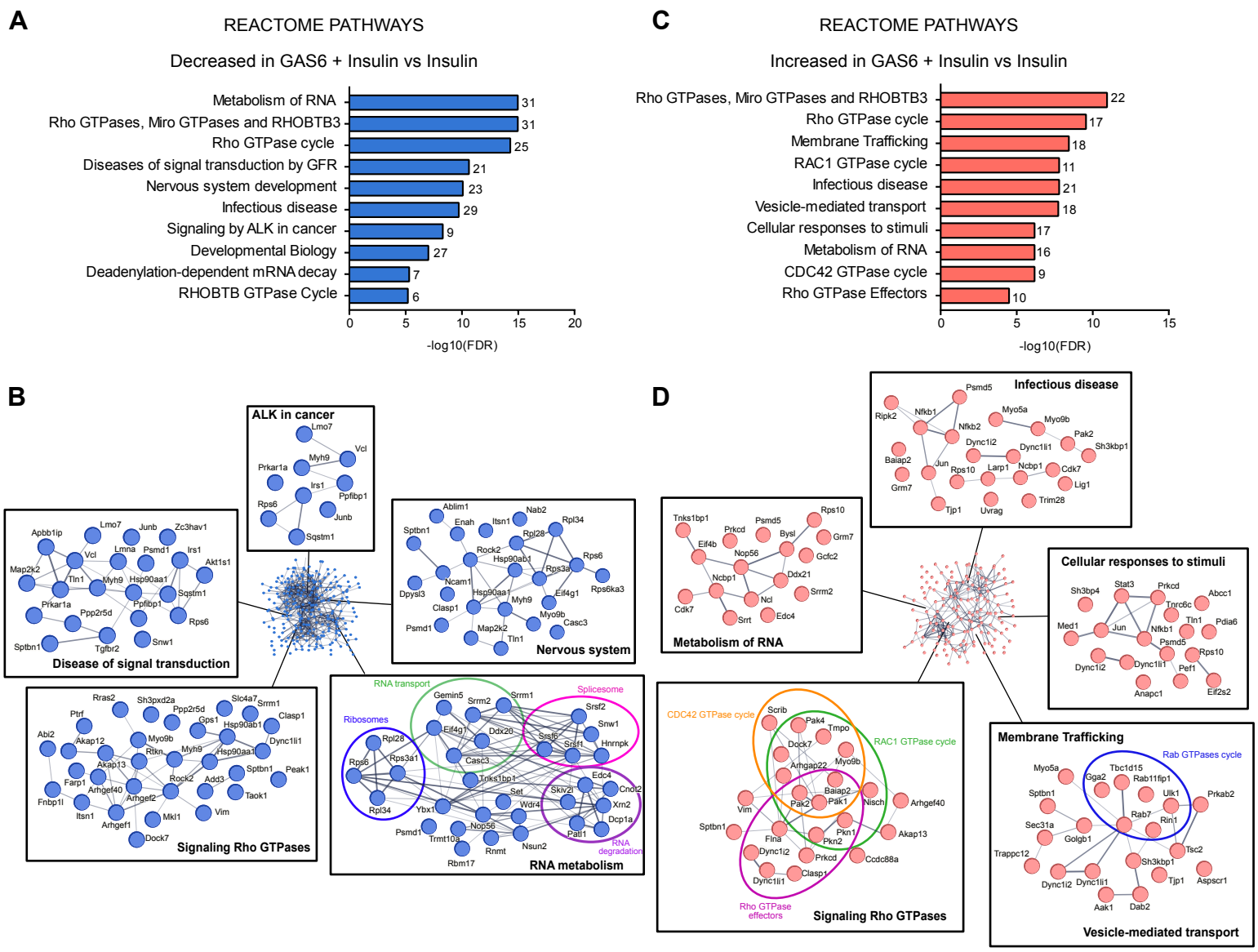
A
REACTOME PATHWAYS
Decreased in GAS6 + Insulin vs Insulin
Metabolism of RNA 31
Rho GTPases, Miro GTPases and RHOBTB3 31
Rho GTPase cycle 25
Diseases of signal transduction by GFR 21
Nervous system development 23
Infectious disease 29
Signaling by ALK in cancer 9
Developmental Biology 27
Deadenylation-dependent mRNA decay 7
RHOBTB GTPase Cycle 6
0 5 10 15 20
-log10(FDR)
C
REACTOME PATHWAYS
Increased in GAS6 + Insulin vs Insulin
Rho GTPases, Miro GTPases and RHOBTB3 22
Rho GTPase cycle 17
Membrane Trafficking 18
RAC1 GTPase cycle 11
Infectious disease 21
Vesicle-mediated transport 18
Cellular responses to stimuli 17
Metabolism of RNA 16
CDC42 GTPase cycle 9
Rho GTPase Effectors 10
0 5 10 15
-log10(FDR)
B
ALK in cancer
Disease of signal transduction
Nervous system
Signaling Rho GTPases
RNA transport
Splicesome
Ribosomes
RNA degradation
RNA metabolism
D
Infectious disease
Metabolism of RNA
Cellular responses to stimuli
CDC42 GTPase cycle
RAC1 GTPase cycle
Rho GTPase effectors
Signaling Rho GTPases
Membrane Trafficking
Rab GTPases cycle
Vesicle-mediated transport

Figure 7

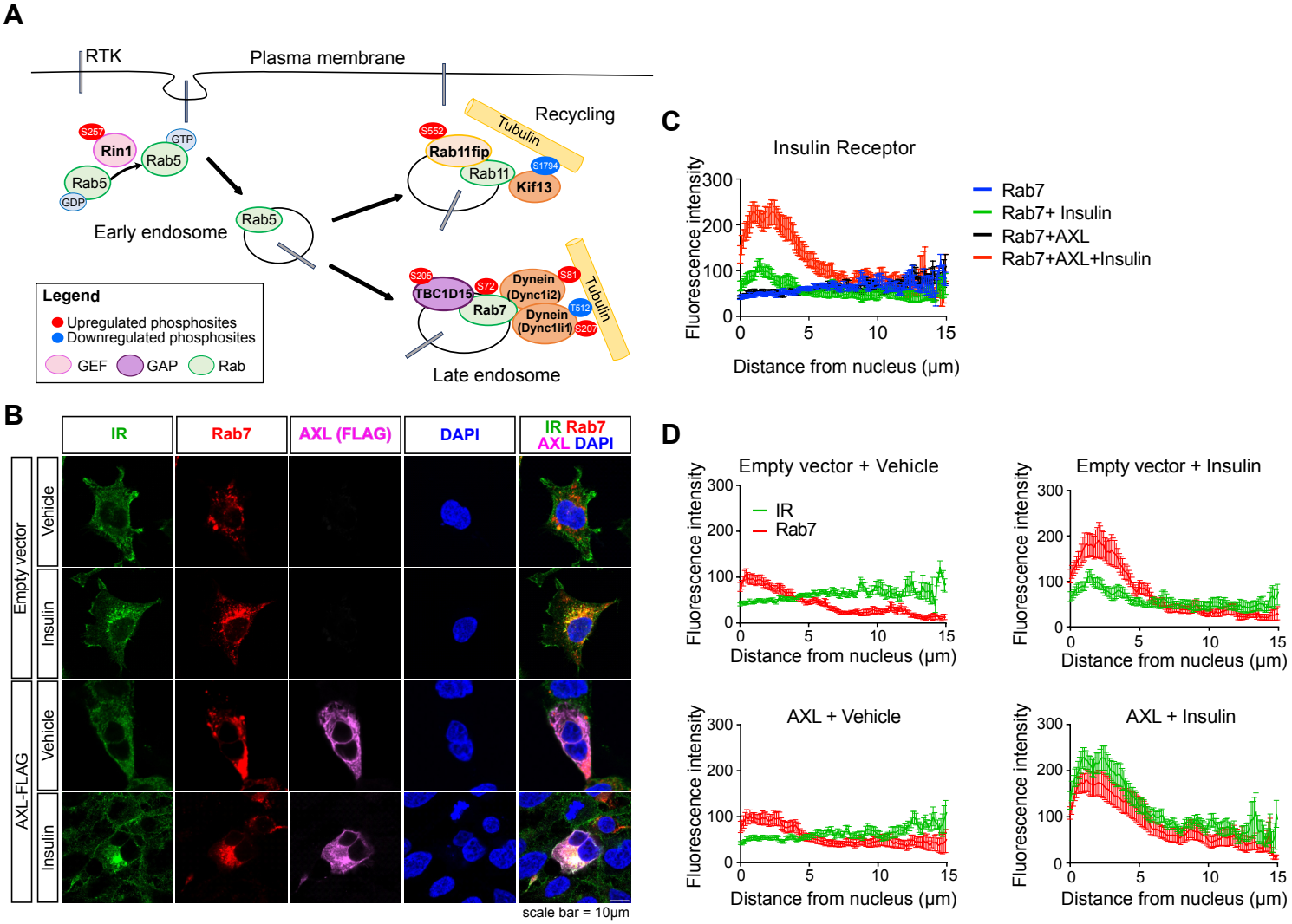
A
RTK
Plasma membrane
Recycling
Tubulin
S257
Rin1
GTP
Rab5
Rab5
GDP
S552
Rab11fip
Rab11
S1794
Kif13
Rab5
Early endosome
S205
TBC1D15
S72
Rab7
Dynein (Dync1i2)
S81
T512
Dynein (Dync1li1)
S207
Tubulin
Late endosome
Legend
Upregulated phosphosites
Downregulated phosphosites
GEF
GAP
Rab
B
IR
Rab7
AXL (FLAG)
DAPI
IR Rab7 AXL DAPI
Empty vector
Vehicle
Insulin
AXL-FLAG
Vehicle
Insulin
scale bar = 10μm
C
Insulin Receptor
Fluorescence intensity
Distance from nucleus (μm)
Rab7
Rab7+ Insulin
Rab7+AXL
Rab7+AXL+Insulin
D
Empty vector + Vehicle
IR
Rab7
Empty vector + Insulin
AXL + Vehicle
AXL + Insulin

Figure 8